Eur. Phys. J. A (2023) 59:60
https://doi.org/10.1140/epja/s10050-023-00975-z

THE EUROPEAN PHYSICAL JOURNAL A

Regular Article - Experimental Physics

Determination of $1p$- and $2p$-stripping excitation functions for $^{16}O+^{142}Ce$ using a recoil mass spectrometer

Rohan Biswas[1,8], S. Nath[1,a], J. Gehlot[1], Gonika[1], Chandra Kumar[1], A. Parihari[2], N. Madhavan[1], A. Vinayak[3], Amritraj Mahato[4], Shoaib Noor[5], Phurba Sherpa[2], Kazuyuki Sekizawa[6,7,b]

[1] Nuclear Physics Group, Inter-University Accelerator Centre, Aruna Asaf Ali Marg, New Delhi 110067, India
[2] Department of Physics and Astrophysics, Delhi University, Delhi 110007, India
[3] Department of Physics, Karnatak University, Dharwad 580003, India
[4] Department of Physics, Central University of Jharkhand, Ranchi 835205, India
[5] School of Physics and Materials Science, Thapar Institute of Engineering and Technology, Patiala 147004, India
[6] Department of Physics, School of Science, Tokyo Institute of Technology, Tokyo 152-8551, Japan
[7] Nuclear Physics Division, Center for Computational Sciences, University of Tsukuba, Ibaraki 305-8577, Japan
[8] *Present Address:* Life Science Division, Diamond Light Source Ltd., Diamond House, Harwell Science and Innovation Campus, Didcot, Oxfordshire OX11 0DE, UK

Received: 26 December 2022 / Accepted: 10 March 2023

Communicated by Takashi Nakamura

Abstract We report the first direct measurement of differential transfer cross sections using a Recoil Mass Spectrometer. Absolute differential $1p$- and $2p$-stripping cross sections at $\theta_{\text{c.m.}} = 180°$ have been determined for the system $^{16}O+^{142}Ce$ by detecting the heavier target-like ions at the focal plane of the Heavy Ion Reaction Analyzer. Focal plane spectra have been compared with the results of a semi-microscopic Monte-Carlo simulation to unambiguously identify the transfer channels. The methodology adopted in this work can be applied to measure multi-nucleon transfer cross sections using other similar recoil separators. The experimental excitation functions for the reactions $^{142}Ce(^{16}O,^{15}N)^{143}Pr$ and $^{142}Ce(^{16}O,^{14}C)^{144}Nd$ have been compared with coupled reaction channels calculations. Shell model calculations have been performed to extract spectroscopic information for the target-like nuclei. An excellent matching between measurement and theory has been obtained for $1p$-stripping. For $2p$-stripping, cluster transfer of two protons has been found to have dominant contribution. Measured transfer probabilities for $1p$- and $2p$-stripping channels have been compared with Time-Dependent Hartree–Fock calculations. Proton stripping channels are found to be more favourable compared to neutron pick-up channels. However, the theory overpredicts the measurement hinting at the need for extended approaches with explicit treatment of pairing correlations in the calculations.

1 Introduction

The simplest picture of a nuclear reaction is a light projectile ion being scattered off a heavier target nucleus. Such a collision, termed as *direct nuclear reaction* is characterized by a very short interaction time $\sim 10^{-22}$ s with active participation of a few nucleons and exchange of few degrees of freedom. In contrast, a *compound nuclear reaction* is much slower in which all the constituent nucleons of the collision partners take part to form a mono-nucleus. The resulting 'compound nucleus' decays by emission of photons and evaporation of light particles. Availability of heavy ion beams made a third and intermediate class of nuclear reactions possible [1]. Such reactions are characterized by creation of binary products in the exit channels with broad mass, charge and angular distributions. Heavy ion-induced reactions, with features intermediate between direct reactions and compound nuclear reactions, had been variously termed as deep inelastic collision, multi-nucleon transfer (MNT), deep-inelastic transfer, quasi-fission, strongly-damped collision and relaxation phenomena by different research groups [2].

Supplementary Information The online version contains supplementary material available at https://doi.org/10.1140/epja/s10050-023-00975-z.

[a] e-mail: subir@iuac.res.in (corresponding author)
[b] e-mail: sekizawa@phys.titech.ac.jp

Published online: 26 March 2023

MNT reactions have been useful for synthesizing nuclides away from the valley of β-stability [3]. A renewed interest in the study of MNT reactions have been ignited by favourable predictions of synthesis of neutron-rich isotopes of heavy elements [4,5] in the recent past. Knowledge about properties of the nuclides in the 'north-east' corner of the nuclear chart, in the vicinity of $N = 126$ shell, is very important for deeper understanding of stellar nucleosynthesis via the r-process. Transfer of nucleons is also known to influence the dynamics of fusion between two heavy nuclei [6,7].

Products of MNT reactions had earlier been identified by chemical separation and measurement of characteristic γ-rays [8]. Magnetic spectrographs of varied configurations [9] had also been used to detect the scattered projectile-like ions from MNT reactions. In the last two decades, a new class of magnetic separators [10–12] with large acceptance, has been put to use in the study of MNT reactions [13–15]. Production of neutron-rich nuclides in damped collisions has been studied recently with novel applications of a few recoil separators which were not originally designed and built for this purpose [16–18]. Production of nuclei far from the stability region in multi-nucleon transfer reactions using a high resolution magnetic spectrometer has also been reported recently [19].

In MNT reactions, either the projectile-like or the target-like ions can be detected at the focal plane of a recoil separator [20]. In most separators, usually the lighter projectile-like ions are detected in the forward angles in the laboratory frame of reference. Mass and charge of the corresponding target-like ions can then be deciphered from two-body collision kinematics. Conversely, the heavier target-like ions may also be detected at the forward angles. This technique was first successfully used in the measurement of sub-barrier transfer reactions for ^{58}Ni+^{A}Sn [21,22] using the Daresbury recoil mass separator [23]. Target-like nuclei, separated according to their mass (A) to charge state (q) ratio, $\left(\frac{A}{q}\right)$, were detected by a position-sensitive detector at the focal plane of the separator. Rehm [8] pointed out that such a device had very limited dynamic range in velocity and charge acceptances. However, the excellent mass resolution made them quite useful in studying MNT reactions. Similar method was adopted for measurement of MNT probability, especially at sub-barrier energies, using other recoil mass spectrometers (RMSs) [24–26]. The Heavy Ion Reaction Analyzer (HIRA) [27], the first generation RMS at IUAC, New Delhi had also been employed to measure few nucleon transfer probabilities in several medium-heavy systems [28–33]. All these measurements suffered from two major drawbacks. Firstly, while estimating the transfer probability, it had been assumed that the elastic channel and all transfer channels had the same efficiency for transmission (ϵ) [34] to the focal plane of the RMS. Secondly, differential transfer cross sections had not been extracted from the data in most cases, as ϵ for quasi-elastic channels had not been known. Differential $1n$- and $2n$-transfer cross sections had been extracted for a limited number of reactions [21,22,24] with the additional assumption that the sum of differential elastic, inelastic and transfer cross sections was equal to the differential Rutherford scattering cross section at energies near and below the Coulomb barrier. Biswas et al. recently reported a methodology [35,36] to overcome these assumptions and *measure* differential quasi-elastic scattering cross sections in an RMS. Besides being useful for the study of MNT reactions, this methodology can also be employed to extract fusion barrier distribution by measuring quasielastic excitation function at $\theta_{\text{c.m.}} = 180°$.

In this article, we report the first direct measurement of differential transfer cross sections using an RMS. Differential cross sections for the reactions ^{142}Ce(^{16}O,^{15}N)^{143}Pr and ^{142}Ce(^{16}O,^{14}C)^{144}Nd have been extracted from yields recorded in the experiment. Details of the experiment are narrated in Sect. 2. We present results of our measurement in Sect. 3. Coupled Reaction Channel (CRC) and Time-Dependent Hartree–Fock (TDHF) calculations, are described in Sects. 4 and 5, respectively. Finally, in Sect. 6, we summarize and conclude our work.

2 The experiment

The experiment has been performed in two runs with a pulsed beam of ^{16}O ions, having a pulse separation of 4 μs, accelerated through the 15UD Pelletron accelerator at IUAC, New Delhi. Isotopically enriched ^{142}Ce target films of thickness 122 μg/cm^2 (with 5% uncertainty) [37], sandwiched between two layers ($\sim$20 μg/cm^2 backing and $\sim$5 μg/cm^2 capping) of graphite films have been used as the target. The targets also contained $\sim$ 7% impurity of ^{140}Ce, which had been verified experimentally [37]. Beam energy (E_{lab}) has been varied between 57–69 MeV, with an intensity between 1–2 particle nanoamperes (pnA). Two solid state silicon detectors, each with a circular aperture of 1 mm diameter, have been placed at $\theta_{\text{lab}} = 15°$ in the horizontal plane at a distance of 100 mm from the target. These detectors have been used as beam monitors during the experiment and for normalization of cross-sections. The HIRA has been kept at $\theta_{\text{lab}} = 0°$ with an opening aperture of 5 msr, corresponding to an angular acceptance $\simeq 2.2°$. A thin ($\sim$ 10 μg/cm^2) graphite foil has been placed 10 cm downstream from the target to reset charge states of the reaction products to equilibrium distribution. A Multi-Wire Proportional Counter (MWPC) of dimensions 150 mm in x and 50 mm in y has been placed at the focal plane of the HIRA. Here, $x - z$ and $y - z$ denote the dispersive and the non-dispersive planes of the RMS, respectively, with z being direction of the beam. Target-like ions, originating from quasi-elastic reactions, have been detected at the focal plane of the HIRA, spatially separated according

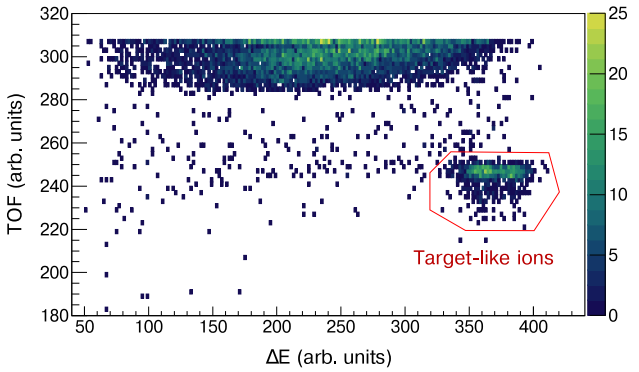

Fig. 1 Scatter plot between ΔE and TOF of the events recorded at the focal plane of the HIRA for ^{16}O+^{142}Ce at $E_{\rm lab} = 63$ MeV. The target-like ions are marked

to their $\frac{A}{q}$. Energy loss (ΔE) information has been obtained from the cathode of the MWPC. A Time-to-Amplitude Converter (TAC) has been set up to measure time-of-flight (TOF) of the ions through the HIRA, in which the anode signal from the MWPC and the radio-frequency (0.25 MHz RF) signal used for beam pulsing have been the start and the stop pulses, respectively.

Figure 1 shows the ΔE-TOF spectrum of the events detected at the focal plane of the HIRA at $E_{\rm lab} = 63$ MeV. Target-like ions have been identified by their higher ΔE and closely-related TOF. The χ-TOF spectrum at the same $E_{\rm lab}$, gated with these events, are shown in Fig. 2a. Ions belonging to two charge states i.e., 14^+ and 15^+ have been detected within the dimensions of the MWPC. The most intense group with $\frac{A}{q} = \frac{142}{14}$ corresponds to elastically/inelastically scattered ^{142}Ce ions. The second group of target-like nuclei from the elastic / inelastic channel(s), marked with $\frac{142}{15}$, can be seen in the extreme left of the figure. It is important to note here that we can not differentiate the inelastic channel(s) from the elastic channel in our method of measurement. Origin of the group marked with $\frac{140}{14}$ is ambiguous. These ions may arise from elastic / inelastic scattering between the projectile nuclei and nuclei of ^{140}Ce, present as impurities in the target film [37]. Probable pickup of two neutrons from ^{142}Ce ($Q_0^{+2n} = -0.41$ MeV) may also lead to formation of ^{140}Ce. Target-like ions, corresponding to probable $1n$-pickup ($Q_0^{+1n} = -3.03$ MeV) channel, have not been identified as a distinct group in the χ-TOF spectrum. The groups marked with $\frac{143}{14}$ and $\frac{144}{14}$ corresponding to one-proton ($1p$) stripping ($Q_0^{-1p} = -6.303$ MeV) and two-proton ($2p$) stripping ($Q_0^{-2p} = -8.54$ MeV) channels, however, can be distinctly observed. While the recoiling target-like nuclei from $1p$-stripping channel (^{143}Pr), have been recorded over the entire range of projectile energies, the same from $2p$-stripping channel, (^{144}Nd), have been observed only at a few energies near the barrier, within the limited duration that have

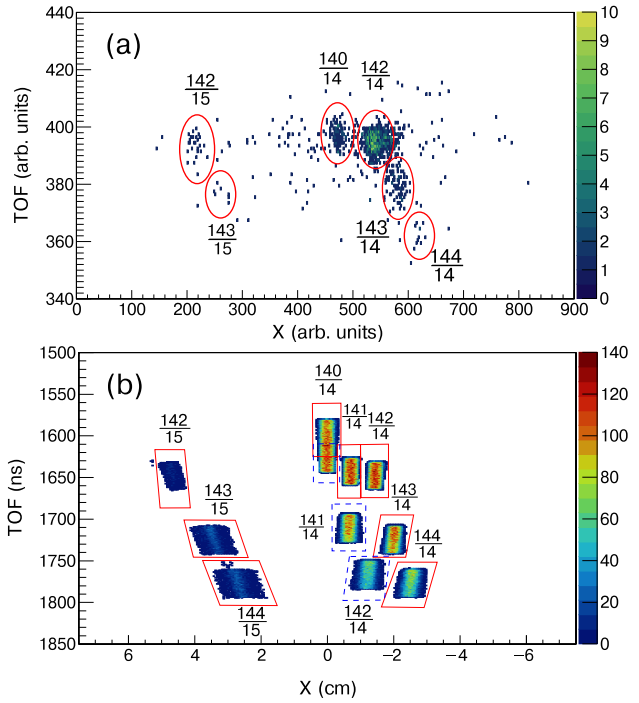

Fig. 2 **a** Experimental and **b** simulated χ-TOF spectra of target-like ions for the system ^{16}O+^{142}Ce at $E_{\rm lab} = 63$ MeV. The identified channels are marked in panel **a**. In panel **b**, position of events from the elastic, $1n$- and $2n$-pickup and $1p$- and $2p$-stripping channels for the system ^{16}O+^{142}Ce are marked within boxes with solid (red) lines. Position of events from the elastic, $1p$- and $2p$-stripping channels for the system ^{16}O+^{140}Ce are also shown in panel **b** and marked within boxes with dashed (blue) lines. See text for details

been available for collecting the data. It must be stated here that ascertaining the charge of the transferred nucleon(s) from the spectrum (Fig. 2a) alone is not possible. Identification of transfer channels have been realized with recourse to Q-value considerations.

Some residual background events, originating from multiple-scattering of projectile ions inside the spectrometer, can be observed in the measured χ-TOF spectrum. Further rejection of background events can be achieved by making use of the method of kinematic coincidence between the recoiling target-like ions detected at the focal plane of the RMS and the back-scattered projectile-like ions detected by a $\Delta E - E$ telescope [31].

3 Results

The elastic/inelastic and transfer channels in the experimental spectrum (Fig. 2a) have been identified based on their $\frac{A}{q}$ values. To rule out any ambiguity in channel identification, the experimental spectrum has been further compared with a simulated χ-TOF spectrum, which is shown in Fig. 2b. The simulation has been carried out by a semi-microscopic Monte

Carlo code [35,36]. It may be noted here that a fixed number (300,000) of events has been considered for the simulation of each channel. Transfer cross sections have not been fed as inputs to the simulation and its purpose is limited to knowing the relative positions of events from the different reaction channels in the χ-TOF plot. Simulated positions of the target-like ions, generated for the system ^{16}O+^{142}Ce, viz. ^{142}Ce (elastic/inelastic), ^{141}Ce (1n-pickup), ^{140}Ce (2n-pickup), ^{143}Pr (1p-stripping) and ^{144}Nd (2p-stripping), are marked in Fig. 2b. In addition, simulated positions of target-like ions which may result from collisions between ^{16}O and ^{140}Ce (impurity in the target film), viz. ^{140}Ce (elastic/inelastic), ^{141}Pr (1p-stripping) and ^{142}Nd (2p-stripping), are also marked in the figure. Comparing the two panels of Fig. 2, we may conclude that (i) the target-like ions resulting from 1n-pickup in the system ^{16}O+^{142}Ce (marked $\frac{141}{14}$ in the top half of panel (b)) can be distinguished from the elastic/inelastic products, if produced in the experiment, (ii) the two probable sources of the group with $\frac{A}{q} = \frac{140}{14}$ can not be resolved in TOF, (iii) the identification of 1p- and 2p-stripping channels for the system ^{16}O+^{142}Ce is unambiguous and (iv) the target-like ions resulting from 1p- and 2p-stripping in the system ^{16}O+^{140}Ce (marked $\frac{141}{14}$ and $\frac{142}{14}$ in the bottom half of panel (b)) should be identifiable, if produced in the experiment. This comparison underlines the need for highly-enriched isotopic targets for such studies with RMSs. We have further verified that the measured yield of $\frac{140}{14}$ group is $\sim$ 8% of the same of $\frac{142}{14}$ group. Thus, the predominant origin of the group $\frac{140}{14}$ appears to be the impurity of ^{140}Ce in the target film.

The absolute differential cross-sections for 1p- and 2p-stripping at centre of mass (c.m.) angle, $\theta_{\text{c.m.}} = 180°$ have been calculated using the relation [36]:

$$\left(\frac{d\sigma}{d\Omega}\right)^{1p(2p)}_{180°} = \frac{Y_{143(144)}}{Y^{\text{Ruth}}_{\text{norm}}} \frac{\Omega_{\text{norm}}}{\Omega^{\text{eff}}_{\text{HIRA}}} \frac{1}{\epsilon_{\text{HIRA}}} \left(\frac{d\sigma}{d\Omega}\right)^{\text{Ruth}}_{\theta_{\text{norm}}} \quad (1)$$

where $Y_{143(144)}$ is the yield of the $\frac{143}{q}$ $\left(\frac{144}{q}\right)$ group(s) in the χ-TOF spectrum (Fig. 2) corresponding to 1p-stripping (2p-stripping). $Y^{\text{Ruth}}_{\text{norm}}$ is the geometric mean of the counts recorded in the two normalization detectors. Ω_{norm} and $\left(\frac{d\sigma}{d\Omega}\right)^{\text{Ruth}}_{\theta_{\text{norm}}}$ are the solid angle subtended by each of the normalization detectors and the differential Rutherford scattering cross section in the c.m. frame of reference at $\theta_{\text{norm}} = 16.32°$ (corresponding to $\theta_{\text{lab}} = 15°$), respectively. The transmission efficiency ϵ_{HIRA} for the target-like ions have been calculated [35] by taking the ratio of the counts of ions reaching the focal plane to the number of ions entering the entrance aperture of the HIRA. The effective solid angle, $\Omega^{\text{eff}}_{\text{HIRA}}$, has been determined experimentally by recording the target-like ions at $E_{\text{lab}} = 48$ MeV using the relation [36]:

$$\Omega^{\text{eff}}_{\text{HIRA}} = \frac{Y^{\text{Ruth}}_{142}}{Y^{\text{Ruth}}_{\text{norm}}} \Omega_{\text{norm}} \frac{1}{\epsilon_{\text{HIRA}}} \left(\frac{d\sigma}{d\Omega}\right)^{\text{Ruth}}_{\theta_{\text{norm}}} \Big/ \left(\frac{d\sigma}{d\Omega}\right)^{\text{Ruth}}_{180°}. \quad (2)$$

At this energy ($\simeq$ 25% below the Coulomb barrier), all scattering events obey Rutherford scattering and the transfer channels are closed. The absolute differential cross sections for 1p- and 2p-stripping channels, as a function of the energy available in the c.m. frame of reference ($E_{\text{c.m.}}$) are, respectively, shown in Figs. 3 and 4.

Error bars in Figs. 3 and 4 include statistical as well as systematic uncertainties, the latter of which are listed in Table

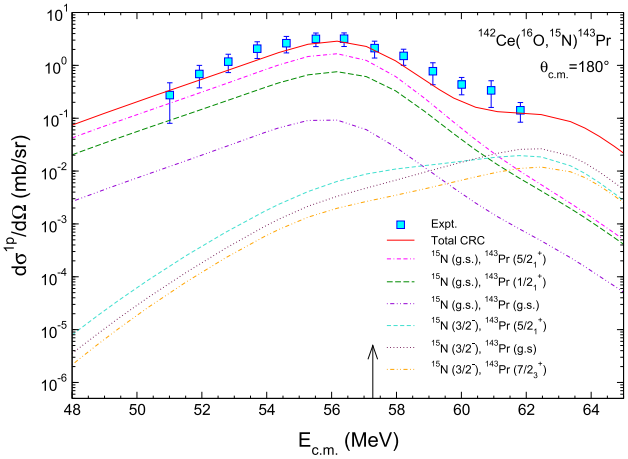

Fig. 3 Absolute differential cross sections for the reaction ^{142}Ce(^{16}O,^{15}N)^{143}Pr at $\theta_{\text{c.m.}} = 180°$ as a function of $E_{\text{c.m.}}$. The full CRC calculation is shown by the solid (red) line. Contributions of different exit channels to the transfer cross sections are also shown. The arrow denotes location of the Coulomb barrier. See text for details

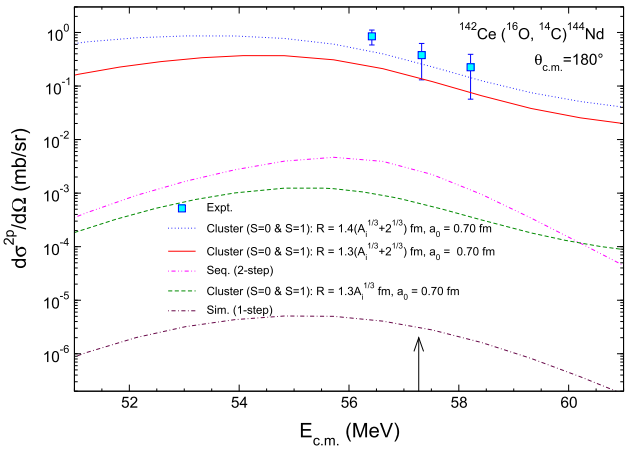

Fig. 4 Absolute differential cross sections for the reaction ^{142}Ce(^{16}O,^{14}C)^{144}Nd at $\theta_{\text{c.m.}} = 180°$ as a function of $E_{\text{c.m.}}$. Results from sequential (two-step), microscopic simultaneous (one-step) and cluster transfer are shown. The arrow denotes location of the Coulomb barrier. See text for details

Table 1 Systematic errors considered while extracting the experimental differential $1p$- and $2p$-stripping cross-sections

Quantity	Uncertainty	% effect
θ_{norm}	0.5°	12.8 [a]
Ω_{norm}	2.0 mm [b]	4.0
	0.01 mm [c]	
ϵ_{HIRA}	10.0 %	10.0
$\Omega^{\text{eff}}_{\text{HIRA}}$	17.1 %	17.1

[a]Error in calculated $\left(\frac{d\sigma}{d\Omega}\right)^{\text{Ruth}}_{\theta_{\text{norm}}}$
[b]Uncertainty in distance between target and detector
[c]Uncertainty in aperture diameter

1. The error in $\Omega^{\text{eff}}_{\text{HIRA}}$ contains statistical uncertainties in the measured yields (Y^{Ruth}_{142} and $Y^{\text{Ruth}}_{\text{norm}}$) at $E_{\text{lab}} = 48$ MeV and similar systematic uncertainties.

4 Coupled reaction channel calculations

Measured differential cross sections have been compared with finite-range CRC model calculations performed using the code FRESCO [38,39]. Structure information for the target-like nuclei, viz., ^{142}Ce, ^{143}Pr and ^{144}Nd have been extracted from large-scale shell model calculations using the code NuShellX [40,41] within `jj56pn` model space and `jj56pna` as the effective interaction [42,43]. Details of the calculations and values of spectroscopic quantities, along with their comparison with experimental values, are provided in the Supplementary Material. The coupling schemes for the projectile-like nuclei, viz., ^{16}O, ^{15}N and ^{14}C and the target-like nuclei, viz., ^{142}Ce, ^{143}Pr and ^{144}Nd are shown in Fig. 5. Entrance channel, exit channel and core-core (^{15}N+^{142}Ce) interactions for $1p$-stripping channel have been defined by optical potential containing real and imaginary parts, taken in Woods–Saxon shape, where the parameters have been determined using Akyüz–Winther formalism [44]. The real parameters have been determined at $E_{\text{lab}} = 63$ MeV. The binding potential for p+^{15}N and p+^{142}Ce reactions have been taken in Woods Saxon form from Ref. [45]. The radius and the diffuseness parameters for p+^{15}N have been taken as 1.26 fm and 0.7 fm, respectively, while 1.3 fm and 0.7 fm have been considered as the values of these parameters, respectively, for p+^{142}Ce. Depth of the real part of bound-state potentials has been varied to reproduce the binding energy of a proton to the core. Spectroscopic Amplitudes (S.A.s) for the $1p_{\frac{1}{2}}$ ground state (g.s.) and the $1p_{\frac{3}{2}}$ third excited state of ^{15}N have been taken to be 1.129 and 1.431, respectively [46]. S.A.s for the overlaps between states in the target-like nuclei are presented in Table 2 of the Supplementary Material. The calculations have been performed in prior representation

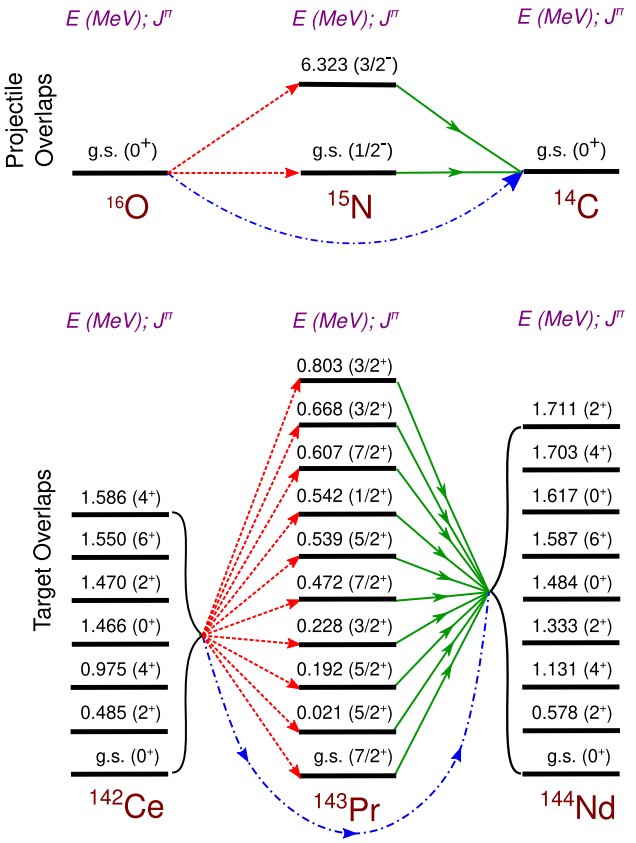

Fig. 5 Coupling schemes adopted for CRC calculations of $1p$- (red dashed arrows) and $2p$-stripping (green solid arrows for two-step and blue dash-dotted arrows for one-step) channels of the system ^{16}O+^{142}Ce for the projectile-like (upper panel) and the target-like (lower panel) nuclei

including full complex remnant terms. The parameters of the optical potential, used in the calculations, are listed in Table 2.

Results of CRC calculations for $1p$-stripping are shown in Fig. 3. Using the potential parameters described above, the theoretical calculation is able to reproduce the experimental excitation function convincingly. The major peak in the excitation function at $E_{\text{c.m.}} \simeq 56$ MeV appears mainly due to transfer of a proton to two excited states of ^{143}Pr, while the projectile-like ^{15}N remains in the g.s. It can also be observed that another peak at $E_{\text{c.m.}} \simeq 63$ MeV, which lies above the Coulomb barrier, results when ^{15}N is left in the $\frac{3}{2}^-$ excited state. Figure 3 shows only those states which contribute to a significant degree to the theoretical cross sections.

To understand the mechanism of $2p$-stripping, CRC calculations have been performed considering (a) sequential transfer (two-step), (b) microscopic simultaneous transfer (one-step) processes and (c) cluster transfer. Couplings considered in the sequential and microscopic simultaneous processes for the projectile-like and the target-like nuclei are shown in Fig. 5.

For $2p$-sequential transfer, the intermediate nuclei have been taken to be the same as that for $1p$-stripping. Global

Table 2 Optical potential parameters used in CRC calculations to define interaction between different channels. Depth (V_0) of the real part of the potential is taken at $E_{\rm lab} = 63$ MeV. Other symbols have their usual meanings

System	V_0 (MeV)	r_0 (fm)	a_0 (fm)	W_0 (MeV)	r_w (fm)	a_w (fm)
^{16}O+^{142}Ce	61.859	1.2	0.651	50.0	1.0	0.4
^{15}N+^{143}Pr	59.571	1.2	0.647	14.893	1.0	0.4
^{15}N+^{142}Ce	59.387	1.2	0.649	14.847	1.2	0.649
^{14}C+^{144}Nd	57.070	1.2	0.647	14.267	1.2	0.647
^{14}C+^{143}Pr	56.893	1.2	0.647	14.223	1.2	0.647
^{14}C+^{142}Ce	56.714	1.2	0.647	14.178	1.2	0.647

optical model parameters have been used for the ^{14}C+^{144}Nd exit channel and ^{14}C+^{143}Pr core-core interaction, as tabulated in Table 2. The proton binding potential has been adopted from Ref. [45], as described in case for $1p$-stripping. The depth of the real part has been adjusted to reproduce the $1p$ binding energies to the ^{14}C and ^{143}Pr cores. S.A.s of 0.9141 and 0.2867, respectively, have been used for the overlaps $\left\langle {}^{15}\mathrm{N}(\frac{1}{2}^-)\middle|{}^{14}\mathrm{C}(0^+)\right\rangle$ and $\left\langle {}^{15}\mathrm{N}(\frac{3}{2}^-)\middle|{}^{14}\mathrm{C}(0^+)\right\rangle$ [47]. S.A.s for overlaps between ^{143}Pr and ^{144}Nd are presented in Table 3 in the Supplementary Material. The calculations have been performed in prior-post combination to avoid the non-orthogonality terms. Results from the CRC $2p$ sequential transfer calculations underpredict the data by more than two orders of magnitude near the barrier, as shown in Fig. 4.

The same interaction potentials have been used in the microscopic simultaneous transfer calculation. The g.s. of ^{14}C has been taken as [47]:

$$\left|{}^{14}\mathrm{C}_{\mathrm{g.s.}}\right\rangle = 0.914\left(1p_{\frac{1}{2}}\right)^{-2}\otimes\left|{}^{16}\mathrm{O}_{\mathrm{g.s.}}\right\rangle + 0.405\left(1p_{\frac{3}{2}}\right)^{-2}\otimes\left|{}^{16}\mathrm{O}_{\mathrm{g.s.}}\right\rangle. \quad (3)$$

In this case, depth of the binding potential has been adjusted to reproduce half the $2p$ separation energies. The calculations have been performed in prior form. In both the above methods, full complex remnant terms have been included in the calculations. The S.A.s for the target-like states, extracted from shell model calculation using `jj56pna` interaction, are shown in Table 4 of the Supplementary Material. The results underpredict the experimental data by six orders of magnitude, as shown in Fig. 4.

In the cluster model [48] analysis, both the anti-symmetric (intrinsic spin of the $2p$-cluster, $S = 0$) and symmetric ($S = 1$) configurations have been considered for the $2p$ pair. In the harmonic oscillator potential, the principal quantum number and orbital angular momentum of individual protons ($n_{\rm i}$, $l_{\rm i}$; $i = 1, 2$) are transformed into (n, l) and (N, L), corresponding parameters relative to each other and to the c.m. of the core-cluster system, respectively. They are related through energy conservation by [49]:

$$\sum_{i=1,2} 2n_i + l_{\rm i} = 2N + L + 2n + l. \quad (4)$$

The proton pair in the ^{14}C core has been assumed to be in both $1s$ ($n = 1$, $l = 0$) and $1p$ ($n = 1$, $l = 1$) states, whereas in the target-like ^{142}Ce core, the proton pair has been considered only in the $1s$ state. We can find the combination of (N, L) using Eq. (4) to define the transfer of angular momentum according to the overlaps. For both the projectile-like and the target-like nuclei, these parameters, along with the cluster S.A.s, are provided in Table 4 of the Supplementary Material. The cluster S.A.s in the LS coupling scheme have been calculated by transforming the $2p$ S.A.s in the $j-j$ coupling scheme using the relation provided in Ref. [50]. The $2p$ Woods–Saxon binding potential well has been defined by $r_0 = 1.3$ fm and $a_0 = 0.7$ fm, while depth of the potential has been adjusted to reproduce the $2p$ separation energies. The calculations have been performed in prior-form in which full complex remnant terms have been included. As observed in Fig. 4, the shape of the excitation function is similar to that obtained from microscopic simultaneous transfer. However, the calculation underpredicts the data by nearly three orders of magnitude near the barrier. It has been observed that changing the radius from $R = 1.3A_{\rm i}^{\frac{1}{3}}$ to $R = 1.3(2^{\frac{1}{3}} + A_{\rm i}^{\frac{1}{3}})$ leads to enhancement of the cross sections by more than two orders of magnitude. Here, $A_{\rm i}$ stands for mass number of the core nucleus. Such observations have been reported in case of two-nucleon transfer earlier (see e.g. Ref. [51]). It has been found that transitions of the $2p$-cluster from the g.s. of ^{16}O to the g.s. and the 4_2^+ excited state of ^{144}Nd have major contributions to calculated cross sections. Further, increasing the radius parameter to $r_0 = 1.4$ fm has resulted in more enhancement of the theoretical cross-sections and better matching with the data. A recent report [52] has also pointed to the role of proton-proton correlations in $2p$-stripping in an intermediate mass system and the difficulty in reproducing $2p$-transfer probability by semi-classical theory. More data points with lesser uncertainty are clearly needed to make more definitive con-

clusions about the mechanism of $2p$-stripping in the present system.

As has been mentioned earlier, populated states of the reaction products cannot be identified in the present method of studying the MNT channels, by identification of mass number (A) at the focal plane of the spectrometer. Additional measurement of characteristic γ-rays would be necessary to overcome this limitation. We must also take note of another probable source of mismatch between measured and calculated cross sections. Particle unbound states of target-like nuclei, if formed in the reaction, would decay immediately and add to the flux of a different channel. For example, ^{144}Nd nuclei, formed at an excitation energy beyond ^{143}Pr+p threshold of 7.969 MeV, would decay in-flight and add to the yield of the $1p$-stripping channel instead of the same for the $2p$-stripping channel. Such possibilities have not been taken care of in the CRC calculations. One has to, therefore, exercise caution while comparing experimental data with CRC results.

5 Time-dependent Hartree–Fock calculations

We have also analyzed the ^{16}O+^{142}Ce reaction based on the microscopic framework of the Time-Dependent Hartree–Fock (TDHF) theory. A three-dimensional (3D) parallel TDHF code has been used, which has been continuously developed and applied for a variety of systems (see Ref. [53] and references therein), including various extensions going beyond the standard TDHF approach [54–57]. Here we provide information relevant to the present analysis. (For details of the theoretical framework and various applications, see, e.g., recent reviews [53,58,59].)

For the energy density functional (EDF), Skyrme SLy4d parameter set [60] has been used, which does not involve the c.m. correction in its fitting protocol [61]. Single-particle wave functions are represented by discretizing 3D Cartesian coordinates into a uniform grid with 0.8 fm grid spacing. For static Hartree–Fock calculations, a box of 24^3 fm^3 has been used, while a box of $64 \times 32 \times 24$ fm^3 has been used for time-dependent simulations. The g.s. of doubly-magic ^{16}O is of spherical shape. Since the number of neutrons in $^{142}_{58}$Ce$_{84}$ is close to the $N = 82$ magic number, we have found that it is nearly of spherical shape in its Hartree–Fock g.s. (with a tiny octupole deformation). We set the incident direction and the impact parameter (b) vector parallel to the $-x$ and $+y$ directions, respectively, assigning $x - y$ plane as the reaction plane. Since the deformation of the target nucleus ($\beta_2 = 0.1259$) is small, we consider a single initial orientation of ^{142}Ce, where a non-axial quadrupole moment, $Q_{22} \propto \langle x^2 - y^2 \rangle$, takes the smallest value in the reaction plane.

Once the EDF is fixed, the TDHF approach does not have adjustable parameters on reaction dynamics. In this sense, TDHF provides a non-empirical description of low-energy heavy-ion reactions. However, it is of course not a perfect framework since, e.g., it misses pairing correlations and mean-field fluctuations. Apart from the uncertainty inherent in the choice of an EDF, disagreements between TDHF and measurements could indicate importance of the physics beyond the TDHF approach. Keeping these points in mind, we compare the TDHF results with the experimental data for the ^{16}O+^{142}Ce reaction.

Since the measurement has been carried out at $\theta_{\text{c.m.}} = 180°$, TDHF calculations have been performed for head-on collisions (i.e., $b = 0$) between ^{16}O and ^{142}Ce, with changing collision energies. One should note that the relative motion of colliding nuclei (mean fields) is classical in TDHF. Hence, one can observe either fusion or non-fusion (not a superposition of them) depending on the initial conditions. For the present reaction at $b = 0$, we have found that $E_{\text{c.m.}} \leq 56.6$ MeV results in binary reactions, whereas fusion takes place for $E_{\text{c.m.}} \geq 56.7$ MeV.

For the binary reactions, we find that transfer of protons is more favorable than that of neutrons, although the absolute values are small. For instance, the average number of transferred protons reaches about 0.86 at the maximum for $E_{\text{c.m.}} = 56.6$ MeV, while that of neutrons is rather small, less than 0.06 at the maximum. From a TDHF wave function after collision, one can extract transfer probabilities using the particle-number projection technique [62]. The extracted probabilities for quasi-elastic [$(0p, 0n)$, without nucleon transfer], $1p$- stripping ($-1p$) and $2p$-stripping ($-2p$) reactions are shown in Fig. 6 as a function of the distance of the closest approach. The same is defined as

$$D = \frac{Z_{\text{p}} Z_{\text{t}} e^2}{2E_{\text{c.m.}}} \left(1 + \text{cosec}\, \frac{\theta_{\text{c.m.}}}{2}\right) \tag{5}$$

where Z_{p} and Z_{t} are the atomic number of the projectile and the target, respectively, $\theta_{\text{c.m.}}$ is the angle of the projectile-like ions in the c.m. frame of reference and $e^2 = 1.44$ MeV fm. We note that one can obtain D from TDHF time evolution, which gives smaller values especially close to the fusion threshold. However, here we use Eq. 5 for comparison with the experimental data. The experimental transfer probability, for channel α, has been computed using the following relation:

$$P^{\alpha}_{tr} = \frac{Y^{\alpha}/\epsilon^{\alpha}_{\text{HIRA}}}{\sum_{i=142,143,144} Y^{i}/\epsilon^{i}_{\text{HIRA}}}; \alpha \in \{143, 144\}. \tag{6}$$

Here Y^i is the yield of target-like ions for channel i.

As is apparent from Fig. 6, processes are dominated by the quasi-elastic scattering without nucleon transfer i.e. $(0p, 0n)$ in the sub-barrier regime. Because of quantum tunneling of single-particle wave functions, there are small, yet finite

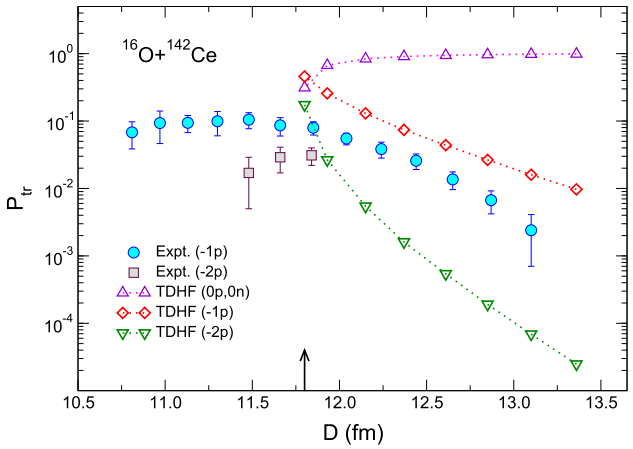

Fig. 6 Transfer probabilities in the ^{16}O+^{142}Ce reaction as a function of D. Experimental data for $1p$ and $2p$ stripping channels are shown by solid symbols. Results of TDHF calculations for quasielastic (0p, 0n), $(-1p)$, and $(-2p)$ channels are shown by open symbols, connected with dotted lines. The arrow indicates distance of the closest approach corresponding to the fusion threshold

probabilities for $1p$- and $2p$-stripping processes. The transfer probabilities increase with increasing $E_{\text{c.m.}}$, since it in turn decreases D. At energy close to the fusion threshold, probabilities of multi-nucleon transfer increase in TDHF as the system develops neck structure, although such behavior is not seen in the experimental data at $E_{\text{c.m.}} \simeq 56.7$ MeV ($D \simeq 11.8$ fm). From the figure, we find that TDHF calculation systematically overestimates P_{tr} for $1p$-stripping (about three times larger) as compared to the measurements. The experimental data indicate that channels accompanying transfer of more than one proton are more probable than the TDHF prediction. However, experimental data for multi-proton transfer are not available in the sub-barrier regime. It is worth mentioning here that total kinetic energy loss (TKEL) is found to be at most 7 MeV for $E_{\text{c.m.}} = 56.6$ MeV within the TDHF approach. Thus, particle evaporation effects are expected to be negligible in the sub-barrier region. It would be interesting to re-examine this reaction employing extended approaches that treat pairing correlations [63–68] explicitly.

6 Conclusions

We demonstrate a novel method to measure differential multi-nucleon transfer cross sections directly, using an RMS. Excitation functions for the reactions ^{142}Ce(^{16}O, ^{15}N)^{143}Pr and ^{142}Ce(^{16}O, ^{14}C)^{144}Nd have been measured around the Coulomb barrier. The heavier target-like ions have been detected at the focal plane of the HIRA, where ions from different exit channels are dispersed according to their $\frac{A}{q}$ values. Information of ΔE and TOF has further helped to reduce the background caused by randomly-scattered projectile-like ions. Ion trajectories inside the RMS have been simulated by a Monte-Carlo code to calculate ϵ for the target-like ions. The channels have been unambiguously identified with the aid of a comparison between measured and simulated χ-TOF spectra. This methodology can be adopted for measuring differential quasi-elastic cross sections, especially for proton transfer channels for which data are scarce, utilizing other similar recoil separators. CRC calculations have been performed to understand the mechanism of $1p$- and $2p$-stripping. Transfer of a proton from g.s. of ^{16}O to excited states of ^{143}Pr contributes significantly to the cross sections near the barrier. Transfer of a cluster of $2p$ from the g.s. of ^{16}O to the g.s. and excited states of ^{144}Nd, with ^{14}C remaining in the g.s., yields reasonable matching with measured cross sections for $2p$-stripping channel. TDHF calculations indicate that transfer of proton(s) is favoured, compared to transfer of neutron(s) in the present reaction. We have found that TDHF calculations overpredict the measured P_{tr} for $1p$-transfer. This could be a signal that multi-proton transfer keeps part of the flux. However, for better understanding, more data for $2p$-transfer and extended approaches of TDHF theory, in which pairing correlations are explicitly taken into account, will be necessary.

Acknowledgements R.B. acknowledges Council of Scientific and Industrial Research (CSIR), New Delhi for financial support via grant no. CSIR/09/760(0030)/2017-EMR-I. K.S. used computational resources of the HPCI system (Oakforest-PACS) provided by Joint Center for Advanced High Performance Computing (JCAHPC) through the HPCI System Project (Project ID: hp210023) and computational resources (in art) of the Yukawa-21 System at Yukawa Institute for Theoretical Physics (YITP), Kyoto University. K.S. was supported by the Japan Society for the Promotion of Science (JSPS) KAKENHI, Grant-in-Aid for Early-Career Scientists via grant no. 19K14704. The authors are grateful to the Pelletron staff of IUAC for excellent operation of the accelerator during the experiment and the Target Laboratory personnel of IUAC for fabrication of targets. Discussions with Dr. Md. Moin Shaikh and Dr. Abhijit Bisoi are thankfully acknowledged.

Data Availability Statement This manuscript has data included as electronic supplementary material. The online version of this article contains supplementary material, which is available to authorized users.

References

1. R. Kaufmann, R. Wolfgang, Nucleon transfer reactions in grazing collisions of heavy ions. Phys. Rev. **121**, 192 (1961)
2. V.V. Volkov, Deep inelastic transfer reactions—the new type of reactions between complex nuclei. Phys. Rep. **44**, 93 (1978)
3. G.G. Adamian, N.V. Antonenko, A. Diaz-Torres, S. Heinz, How to extend the chart of nuclides? Eur. Phys. J. A **56**, 47 (2020)
4. V. Zagrebaev, W. Greiner, Production of new heavy isotopes in low-energy multinucleon transfer reactions. Phys. Rev. Lett. **101**, 122701 (2008)
5. G.G. Adamian, N.V. Antonenko, V.V. Sargsyan, W. Scheid, Predicted yields of new neutron rich isotopes of nuclei with $Z = 64$–80 in the multinucleon transfer reaction ^{48}Ca+^{238}U. Phys. Rev. C **81**, 057602 (2010)

6. C.R. Morton, M. Dasgupta, D.J. Hinde, J.R. Leigh, R.C. Lemmon, J.P. Lestone, J.C. Mein, J.O. Newton, H. Timmers, N. Rowley, A.T. Kruppa, Clear signatures of specific inelastic and transfer channels in the distribution of fusion barriers. Phys. Rev. Lett. **72**, 4074 (1994)
7. G. Pollarolo, Quasielastic barrier distributions: role of particle transfer channels. Phys. Rev. Lett. **100**, 252701 (2008)
8. K.E. Rehm, Quasi-elastic heavy-ion collisions. Annu. Rev. Nucl. Part. Sci. **41**, 429 (1991)
9. H.A. Enge, Magnetic spectrographs for nuclear reaction studies. Nucl. Instrum. Methods **162**, 161 (1979)
10. F. Cappuzzello, C. Agodi, D. Carbone, M. Cavallaroi, The MAGNEX spectrometer: results and perspectives. Eur. Phys. J. A **52**, 167 (2016)
11. M. Rejmund, B. Lecornu, A. Navin, C. Schmitt, S. Damoy, O. Delaune, J. M. Enguerrand, G. Fremont, P. Gangnant, L. Gaudefroy, B. Jacquot, J. Pancin, S. Pullanhiotan, C. Spitaels, Performance of the improved larger acceptance spectrometer: VAMOS++. Nucl. Instrum. Methods Phys. Res. Sect. A **646**, 184 (2011)
12. ...A. Latina, A.M. Stefanini, S. Beghini, B.R. Behera, L. Corradi, G. De Angelis, A. De Rosa, E. Fioretto, A. Gadea, M. Gulmini, G. Inglima, M. LaCommara, G. Maron, R. Menegazzo, N. Marginean, G. Montagnoli, D.R. Napoli, D. Pierroutsakou, G. Pollarolo, M. Romoli, M. Sandoli, F. Scarlassara, S. Szilner, N. Toniolo, M. Trotta, Y.W. Wu, PRISMA—a magnetic spectrometer for heavy ions at LNL. Nucl. Phys. A **734**, E1 (2004)
13. J.L. Ferreira, D. Carbone, M. Cavallaro, N.N. Deshmukh, C. Agodi, G.A. Brischetto, S. Calabrese, F. Cappuzzello, E.N. Cardozo, I. Ciraldo, M. Cutuli, M. Fisichella, A. Foti, L. La Fauci, O. Sgouros, V. Soukeras, A. Spatafora, D. Torresi, J. Lubian, Analysis of two-proton transfer in the ^{40}Ca(^{18}O,^{20} Ne)^{38}Ar reaction at 270 MeV incident energy. Phys. Rev. C **103**, 054604 (2021)
14. Y.X. Watanabe, Y.H. Kim, S.C. Jeong, Y. Hirayama, N. Imai, H. Ishiyama, H.S. Jung, H. Miyatake, S. Choi, J.S. Song, E. Clement, G. de France, A. Navin, M. Rejmund, C. Schmitt, G. Pollarolo, L. Corradi, E. Fioretto, D. Montanari, M. Niikura, D. Suzuki, H. Nishibata, J. Takatsu, Pathway for the production of neutron-rich isotopes around the N = 126 shell closure. Phys. Rev. Lett. **115**, 172503 (2015)
15. F. Galtarossa, L. Corradi, S. Szilner, E. Fioretto, G. Pollarolo, T. Mijatović, D. Montanari, D. Ackermann, D. Bourgin, S. Courtin, G. Fruet, A. Goasduff, J. Grebosz, F. Haas, D. Jelavić Malenica, S.C. Jeong, H.M. Jia, P.R. John, D. Mengoni, M. Milin, G. Montagnoli, F. Scarlassara, N. Skukan, N. Soić, A.M. Stefanini, E. Strano, V. Tokić, C.A. Ur, J.J. Valiente-Dobón, Y.X. Watanabe, Mass correlation between light and heavy reaction products in multinucleon transfer ^{197}Au+^{130}Te collisions. Phys. Rev. C **97**, 054606 (2018)
16. I. Stefan, B. Fornal, S. Leoni, F. Azaiez, C. Portail, J.C. Thomas, A.V. Karpov, D. Ackermann, P. Bednarczyk, Y. Blumenfeld, S. Calinescu, A. Chbihi, M. Ciemala, N. Cieplicka-Oryńczak, F.C.L. Crespi, S. Franchoo, F. Hammache, Ł.W. Iskra, B. Jacquot, R.V.F. Janssens, O. Kamalou, T. Lauritsen, M. Lewitowicz, L. Olivier, S.M. Lukyanov, M. Maccormick, A. Maj, P. Marini, I. Matea, M.A. Naumenko, F. de Oliveira Santos, C. Petrone, Yu.E. Penionzhkevich, F. Rotaru, H. Savajols, O. Sorlin, M. Stanoiu, B. Szpak, O.B. Tarasov, D. Verney, Neutron-rich nuclei produced at zero degrees in damped collisions induced by a beam of ^{18}O on a ^{238}U target. Phys. Lett. B **779**, 456 (2018)
17. A. Di Nitto, J. Khuyagbaatar, D. Ackermann, L.-L. Andersson, E. Badura, M. Block, H. Brand, I. Conrad, D.M. Cox, C.E. Düllmann, J. Dvorak, K. Eberhardt, P.A. Ellison, N.E. Esker, J. Even, C. Fahlander, U. Forsberg, J.M. Gates, P. Golubev, O. Gothe, K.E. Gregorich, W. Hartmann, R.D. Herzberg, F.P. Heßberger, J. Hoffmann, R. Hollinger, A. Hübner, E. Jäger, B. Kindler, S. Klein, I. Kojouharov, J.V. Kratz, J. Krier, N. Kurz, S. Lahiri, B. Lommel, M. Maiti, R. Mändl, E. Merchán, S. Minami, A.K. Mistry, C. Mokry, H. Nitsche, J.P. Omtvedt, G.K. Pang, D. Renisch, D. Rudolph, J. Runke, L.G. Sarmiento, M. Schädel, H. Schaffner, B. Schausten, A. Semchenkov, J. Steiner, P. Thörle-Pospiech, N. Trautmann, A. Türler, J. Uusitalo, D. Ward, M. Wegrzecki, P. Wieczorek, N. Wiehl, A. Yakushev, V. Yakusheva, Study of non-fusion products in the ^{50}Ti+^{249}Cf reaction. Phys. Lett. B **784**, 199 (2018)
18. H.M. Devaraja, S. Heinz, D. Ackermann, T. Göbel, F.P. Heßberger, S. Hofmann, J. Maurer, G. Münzenberg, A.G. Popeko, A.V. Yeremin, New studies and a short review of heavy neutron-rich transfer products. Eur. Phys. J. A **56**, 224 (2020)
19. A.K. Azhibekov, V.A. Zernyshkin, V.A. Maslov, Y.E. Penionzhkevich, K. Mendibayev, T. Issatayev, M.A. Naumenko, N.K. Skobelev, S.S. Stukalov, D. Aznabaev, Differential production cross sections for isotopes of light nuclei in the ^{18}O+^{181}Ta reaction. Phys. Atom. Nucl. **83**, 93 (2020)
20. L. Corradi, G. Pollarolo, S. Szilner, Multinucleon transfer processes in heavy-ion reactions. J. Phys. G Nucl. Part. Phys. **36**, 113101 (2009)
21. R.R. Betts, P.M. Evans, C.N. Pass, N. Poffé, A.E. Smith, L. Stuttgé, J.S. Lilley, D.W. Banes, K.A. Connell, J. Simpson, J.R.H. Smith, A.N. James, B.R. Fulton, Measurement of sub-barrier transfer reactions for ^{58}Ni+Sn using a recoil mass separator. Phys. Rev. Lett. **59**, 978 (1987)
22. C.N. Pass, P.M. Evans, A.E. Smith, L. Stuttgé, R.R. Betts, J.S. Lilley, D.W. Banes, K.A. Connell, J. Simpson, J.R. Smith, A.N. James, B.R. Fulton, Study of neutron transfer reactions at sub-Coulomb energies using a recoil separator. Nucl. Phys. A **499**, 173 (1989)
23. A.N. James, T.P. Morrison, K.L. Ying, K.A. Connell, H.G. Price, J. Simpson, Microsecond mass separation of heavy compound nucleus residues using the Daresbury recoil separator. Nucl. Instrum. Methods Phys. Res. Sect. A **267**, 144 (1988)
24. M.G. Herman, L.L. Lee Jr., R.J. Vojtech, S.B. Gazes, M. Satteson, J. Boyle, Measurements of 180° sub-barrier transfer reaction cross sections in S+Mo,Nb systems, pp. 137–142, Proc. Symp. Heavy Ion Interactions around the Coulomb Barrier, Legnaro, Italy, ed. by C. Signorini et al., Lecture Notes in Physics, Vol. 317 (Springer, Berlin, 1988)
25. R.B. Roberts, S.B. Gazes, J.E. Mason, M. Satteson, S.G. Teichmann, L.L. Lee Jr., J.F. Liang, J.C. Mahon, R.J. Vojtech, Sub-barrier one- and two-neutron pickup measurements in ^{32}S+^{93}Nb,^{98,100}Mo reactions at 180°. Phys. Rev. C **47**, R1831 (1993)
26. D.R. Napoli, A.M. Stefanini, H. Moreno Gonzalez, B. Million, G. Prete, P. Spolaore, M. Narayanasamy, Z.C. Li, S. Beghini, G. Montagnoli, F. Scarlassara, G.F. Segato, C. Signorini, F. Soramel, G. Pollarolo, A. Rapisarda, Sub-barrier transfer reactions of ^{32}S+^{64}Ni. Nucl. Phys. A **559**, 443 (1993)
27. A.K. Sinha, N. Madhavan, J.J. Das, P. Sugathan, D.O. Kataria, A.P. Patro, G.K. Mehta, Heavy ion reaction analyzer (HIRA): a recoil mass separator facility at NSC. Nucl. Instrum. Methods Phys. Res. Sect. A **339**, 543 (1994)
28. D.O. Kataria, A.K. Sinha, J.J. Das, N. Madhavan, P. Sugathan, L.T. Baby, I. Mazumdar, R. Singh, C.V.K. Baba, Y.K. Agarwal, A.M. Vinodkumar, K.M. Varier, One- and two-nucleon transfer in the ^{28}Si+^{68}Zn system at energies below the Coulomb barrier. Phys. Rev. C **56**, 1902 (1997)
29. V. Tripathi, L.T. Baby, P.V. Madhusudhana Rao, S.K. Hui, R. Singh, J.J. Das, P. Sugathan, N. Madhavan, A.K. Sinha, Measurement of the ground state 2n pickup probability for ^{28}Si+^{68}Zn and its role in sub-barrier fusion enhancement. Pramana J. Phys. **53**, 535 (1999)
30. L.T. Baby, V. Tripathi, D.O. Kataria, J.J. Das, P. Sugathan, N. Madhavan, A.K. Sinha, M.C. Radhakrishna, N.M. Badiger, N.G. Puttaswamy, A.M. Vinodkumar, N.V.S.V. Prasad, Transfer and higher-order phonon coupling effects in the sub-barrier fusion of ^{28}Si and ^{93}Nb. Phys. Rev. C **56**, 1936 (1997)

31. A.K. Sinha et al. in collaboration with L.T. Baby, N. Badiger, J.J. Das, S.K. Hui, D.O. Kataria, R.G. Kulkarni, N. Madhavan, P.V. Madhusudhana Rao, I. Majumdar, M.C. Radhakrishna, N.V.S.V. Prasad, N.G. Puttaswamy, P. Shakeeb, R. Singh, D.L. Shastry, P. Sugathan, V. Tripathi, K.M. Varier, A.M. Vinodkumar, Sub-barrier few-nucleon transfer reaction and channel coupling effects in heavy ion fusion. J. Phys. G Nucl. Part. Phys. **23**, 1331 (1997)
32. K.M. Varier, A.M. Vinodkumar, N.V.S.V. Prasad, P.V. Madhusudhana Rao, D.L. Sastry, L.T. Baby, M.C. Radhakrishna, N.G. Puttaswamy, J.J. Das, P. Sugathan, N. Madhavan, A.K. Sinha, D.O. Kataria, Transfer measurements for the Ti + Ni systems at near barrier energies. Pramana J. Phys. **53**, 529 (1999)
33. S. Kalkal, S. Mandal, N. Madhavan, A. Jhingan, E. Prasad, R. Sandal, S. Nath, J. Gehlot, R. Garg, G. Mohanto, M. Saxena, S. Goyal, S. Verma, B.R. Behera, S. Kumar, U.D. Pramanik, A.K. Sinha, R. Singh, Multinucleon transfer reactions for the ^{28}Si+^{90,94}Zr systems in the region below and near the Coulomb barrier. Phys. Rev. C **83**, 054607 (2011)
34. S. Nath, A Monte Carlo code to calculate transmission efficiency of HIRA. Nucl. Instrum. Methods Phys. Res. Sect. A **576**, 403 (2007)
35. R. Biswas, S. Nath, Simulation of a recoil mass spectrometer for measurement of differential quasi-elastic scattering cross sections. Eur. Phys. J. A **56**, 1 (2020)
36. R. Biswas, S. Kalkal, S. Nath, Studying multi-nucleon transfer reaction in a recoil mass spectrometer. Eur. Phys. J A **57**, 9 (2021)
37. R. Biswas, S.R. Abhilash, H. Gupta, G.R. Umapathy, A. Dawar, S. Nath, Fabrication of thin ^{140,142}Ce target foils for study of nuclear reaction dynamics. Vacuum **188**, 110159 (2021)
38. http://www.fresco.org.uk/
39. I.J. Thompson, Coupled reaction channels calculations in nuclear physics. Comput. Phys. Rep. **7**, 167 (1988)
40. W.D.M. Rae, NuShellX. http://www.garsington.eclipse.co.uk/
41. B.A. Brown, W.D.M. Rae, The shell-model code NuShellX@MSU. Nucl. Data Sheets **120**, 115 (2014)
42. J. Hakala, J. Dobaczewski, D. Gorelov, T. Eronen, A. Jokinen, A. Kankainen, V.S. Kolhinen, M. Kortelainen, I.D. Moore, H. Penttilä, S. Rinta-Antila, J. Rissanen, A. Saastamoinen, V. Sonnenschein, J. Äystö, Precision mass measurements beyond ^{132}Sn: anomalous behavior of odd-even staggering of binding energies. Phys. Rev. Lett. **109**, 032501 (2012)
43. K.L. Jones, A.S. Adekola, D.W. Bardayan, J.C. Blackmon, K.Y. Chae, K.A. Chipps, J.A. Cizewski, L. Erikson, C. Harlin, R. Hatarik, R. Kapler, R.L. Kozub, J.F. Liang, R. Livesay, Z. Ma, B.H. Moazen, C.D. Nesaraja, F.M. Nunes, S.D. Pain, N.P. Patterson, D. Shapira, J.F. Shriner Jr., M.S. Smith, T.P. Swan, J.S. Thomas, The magic nature of ^{132}Sn explored through the single-particle states of ^{133}Sn. Nature **465**, 454 (2010)
44. Ö. Akyüz, A. Winther, Proceedings of the International School of Physics "Enrico Fermi", Course LXXVII edited by R.A. Broglia, C.H. Dasso, R. Ricci (North-Holland, Amsterdam, 1981)
45. B. Paes, G. Santagati, R. Magana Vsevolodovna, F. Cappuzzello, D. Carbone, E.N. Cardozo, M. Cavallaro, H. García-Tecocoatzi, A. Gargano, J.L. Ferreira, S.M. Lenzi, R. Linares, E. Santopinto, A. Vitturi, J. Lubian, Long-range versus short-range correlations in the two-neutron transfer reaction ^{64}Ni(^{18}O,^{16}O)^{66}Ni. Phys. Rev. C **96**, 044612 (2017)
46. M. Leuschner, J.R. Calarco, F.W. Hersman, E. Jans, G.J. Kramer, L. Lapikás, G. van der Steenhoven, P.K.A. de Witt Huberts, H.P. Blok, N. Kalantar-Nayestanaki, J. Friedrich, Quasielastic proton knockout from ^{16}O. Phys. Rev. C. **49**, 955 (1994)
47. P.P. Tung, K.A. Erb, M.W. Sachs, G.B. Sherwood, R.J. Ascujtto, D.A. Bromley, Sequential amplitudes in heavy-ion induced two-proton transfer reactions. Phys. Rev. C **18**, 1663 (1978)
48. G.R. Satchler, *Direct Nuclear Reactions* (Oxford University Press, Oxford, 1983)
49. M. Moshinsky, Transformation brackets for harmonic oscillator functions. Nucl. Phys. **13**, 104 (1959)
50. D. Carbone, J.L. Ferreira, F. Cappuzzello, J. Lubian, C. Agodi, M. Cavallaro, A. Foti, A. Gargano, S.M. Lenzi, R. Linares, G. Santagati, Microscopic cluster model for the description of new experimental results on the ^{13}C(^{18}O, ^{16}O)^{15}C two-neutron transfer at 84 MeV incident energy. Phys. Rev. C. **95**, 034603 (2017)
51. V. Jha, B.J. Roy, A. Chatterjee, H.S. Patel, B. Srinivasan, M.G. Betigeri, H. Machner, ^{16}O-induced transfer reactions on ^{90}Zr. Eur. Phys. J. A **15**, 389 (2002)
52. L. Corradi, S. Szilner, G. Pollarolo, T. Mijatović, D. Montanari, E. Fioretto, A. Goasduff, D. Jelavić Malenica, G. Montagnoli, A.M. Stefanini, Evidence of proton-proton correlations in the ^{116}Sn+^{60}Ni transfer reactions. Phys. Lett. B **834**, 137477 (2022)
53. K. Sekizawa, Time-dependent Hartree–Fock theory and its extensions for the multinucleon transfer reactions: a mini review. Front. Phys. **7**, 20 (2019)
54. E. Williams, K. Sekizawa, D.J. Hinde, C. Simenel, M. Dasgupta, I.P. Carter, K.J. Cook, D.Y. Jeung, S.D. McNeil, C.S. Palshetkar, D.C. Rafferty, K. Ramachandran, A. Wakhle, Exploring zeptosecond quantum equilibration dynamics: From deep-inelastic to fusion-fission outcomes in ^{58}Ni+^{60}Ni reactions. Phys. Rev. Lett. **120**, 022501 (2018)
55. K. Sekizawa, K. Hagino, Time-dependent Hartree–Fock plus Langevin approach for hot fusion reactions to synthesize the $Z = 120$ superheavy element. Phys. Rev. C **99**, 051602(R) (2019)
56. K. Sekizawa, S. Ayik, Quantal diffusion approach for multinucleon transfer processes in the ^{58,64}Ni+^{208}Pb reactions: toward the production of unknown neutron-rich nuclei. Phys. Rev. C **102**, 014620 (2020)
57. S. Ayik, K. Sekizawa, Kinetic energy dissipation and fluctuations in strongly-damped heavy-ion collisions within the stochastic mean-field approach. Phys. Rev. C **102**, 064619 (2020)
58. C. Simenel, A.S. Umar, Heavy-ion collisions and fission dynamics with the time-dependent Hartree–Fock theory and its extensions. Prog. Part. Nucl. Phys. **103**, 19 (2018)
59. P.D. Stevenson, M.C. Barton, Low-energy heavy-ion reactions and the Skyrme effective interaction. Prog. Part. Nucl. Phys. **104**, 142 (2019)
60. K.-H. Kim, T. Otsuka, P. Bonche, Three-dimensional TDHF calculations for reactions of unstable nuclei. J. Phys. G Nucl. Part. Phys. **23**, 1267 (1997)
61. E. Chabanat, P. Bonche, P. Haensel, J. Meyer, R. Schaeffer, New Skyrme effective forces for supernovae and neutron rich nuclei. Phys. Scr. **T56**, 231 (1995)
62. C. Simenel, Particle transfer reactions with the time-dependent Hartree–Fock theory using a particle number projection technique. Phys. Rev. Lett. **105**, 192701 (2010)
63. S. Ebata, T. Nakatsukasa, T. Inakura, K. Yoshida, Y. Hashimoto, K. Yabana, Canonical-basis time-dependent Hartree–Fock–Bogoliubov theory and linear-response calculations. Phys. Rev. C **82**, 034306 (2010)
64. G. Scamps, D. Lacroix, Effect of pairing on one- and two-nucleon transfer below the Coulomb barrier: a time-dependent microscopic description. Phys. Rev. C **87**, 014605 (2013)
65. P. Magierski, K. Sekizawa, G. Wlazłowski, Novel role of superfluidity in low-energy nuclear reactions. Phys. Rev. Lett. **119**, 042501 (2017)
66. Y. Hashimoto, G. Scamps, Gauge angle dependence in time-dependent Hartree–Fock–Bogoliubov calculations of ^{20}O+^{20}O head-on collisions with the Gogny interaction. Phys. Rev. C **94**, 014610 (2016)
67. G. Scamps, Y. Hashimoto, Transfer probabilities for the reactions ^{14,20}O+^{20}O in terms of multiple time-dependent Hartree–Fock–Bogoliubov trajectories. Phys. Rev. C **96**, 031602(R) (2017)

68. D. Regnier, D. Lacroix, G. Scamps, Y. Hashimoto, Microscopic description of pair transfer between two superfluid Fermi systems: combining phase-space averaging and combinatorial techniques. Phys. Rev. C **97**, 034627 (2018)